



RESEARCH ARTICLE

Hydrothermal synthesis of chiral carbon dots

Anastasia Visheratina¹  | Leila Hesami² | Ashleigh K. Wilson² |
Nicole Baalbaki¹ | Natalia Noginova² | Mikhail A. Noginov² |
Nicholas A. Kotov¹ 

¹Biointerfaces Institute, University of Michigan, Ann Arbor, Michigan, USA

²Center for Materials Research, Norfolk State University, Norfolk, Virginia, USA

Correspondence

Nicholas A. Kotov, Biointerfaces Institute, University of Michigan, 2800 Plymouth Rd, Ann Arbor, MI 48105, USA.

Email: kotov@umich.edu

Funding information

Vannevar Bush DoD Fellowship, Grant/Award Number: N000141812876; MURI from the Office of Naval Research, Grant/Award Numbers: MURI N00014-20-1-2479, MURI N00014-18-1-2497; DEI Initiative UM College of Engineering; University of Michigan College of Engineering; National Science Foundation (NSF), Grant/Award Numbers: 2112595, 1856515, 1830886, DMR-0420785, DMR-0723032; Michigan Center for Materials Characterization; Air Force Office of Scientific Research (AFOSR), Grant/Award Number: FA9550-18-1-0417; Department of Defense (DoD), Grant/Award Number: W911NF1810472; National Nuclear Security Administration (NNSA), Grant/Award Numbers: DE-NA-0003525, DE-NA0004007; Sandia National Laboratories

Abstract

Nanocolloids that are cumulatively referred to as nanocarbons, attracted significant attention during the last decade because of facile synthesis methods, water solubility, tunable photoluminescence, easy surface modification, and high biocompatibility. Among the latest development in this research area are chiral nanocarbons exemplified by chiral carbon dots (CDots). They are expected to have applications in sensing, catalysis, imaging, and nanomedicine. However, the current methods of CDots synthesis show often contradictory chemical/optical properties and structural information that required a systematic study with careful structural evaluation. Here, we investigate and optimize chiroptical activity and photoluminescence of *L*- and *D*-CDots obtained by hydrothermal carbonization of *L*- and *D*-cysteine, respectively. Nuclear magnetic resonance spectroscopy demonstrates that they are formed via gradual dehydrogenation and condensation reactions of the starting amino acid leading to particles with a wide spectrum of functional groups including aromatic cycles. We found that the chiroptical activity of CDots has an inverse correlation with the synthesis duration and temperature, whereas the photoluminescence intensity has a direct one, which is associated with degree of carbonization. Also, our studies show that the hydrothermal synthesis of cysteine in the presence of boric acid leads to the formation of CDots rather than boron nitride nanoparticles as was previously proposed in several reports. These results can be used to design chiral carbon-based nanoparticles with optimal chemical, chiroptical, and photoluminescent properties.

KEYWORDS

carbon-based nanomaterials, fluorescent carbon dots, hydrothermal synthesis, nanoscale chirality, optical activity

[This article is part of the Special Issue: Chirality Materials.]

This is an open access article under the terms of the [Creative Commons Attribution-NonCommercial-NoDerivs](https://creativecommons.org/licenses/by-nc-nd/4.0/) License, which permits use and distribution in any medium, provided the original work is properly cited, the use is non-commercial and no modifications or adaptations are made.

© 2022 The Authors. *Chirality* published by Wiley Periodicals LLC.

1 | INTRODUCTION

Chiral inorganic nanostructures display exceptionally high chiroptical activity compared to that of organic objects because of their high electrical polarizability, magnetic susceptibility, and importantly, better match in dimensions with visible wavelengths compared to the classical chiral organic molecules, such as amino acids.^{1,2} Exceptional optical, chemical, and physical properties of chiral nanostructures coupled with their protein-mimetic biological activity¹ allow exploration of fundamental questions, such as the origin of homochirality on Earth and chirality transfer.² The presence of helical, tetrahedral, cross-rod and other mirror-asymmetric geometries at multiple scales from angstroms to microns, make nanostructured chiral particles promising chemical compounds for chiral sensing, separation, bioimaging, enantioselective recognition, and chiral catalysis.^{1,3,4} Among all chiral inorganic nanostructures, those based on noble metals (e.g., gold and silver) and II–VI semiconductors (e.g., CdTe and CdSe) nanoparticles (NPs) are the most studied ones.⁵ Carbon-based nanomaterials with mirror asymmetry, including carbon nanotubes,⁶ graphene,⁷ and nanodiamonds,⁸ broaden the spectrum of potential applications of chiral inorganic nanostructures while reducing their toxicity, cost, and environmental concerns. Among them are carbonaceous chiral particles often referred to as carbon dots (CDots) that have gained significant attention during the last decade because they offer a hard-to-find combination of multiple properties: biocompatibility, biodegradability, low toxicity, high colloidal stability, high photostability, bright photoluminescence (PL), spectral tunability, and facile chemical functionalization.⁹ Although their chemical structure contains a lot of unknowns exemplified by the uncertainty about the chemical nature and scale of chiral geometries they possess, these properties allowed CDots to be used in sensors, bioimaging, drug delivery, catalysis, photovoltaics, and optoelectronics.^{10–14}

The extensive studies of nanocarbons for biomedical applications stimulated early works on their chirality.¹⁵ For example, covalent attachment of *L*- or *D*-Cys moieties to the edges of graphene NPs leads to their helical buckling due to chiral interactions at the “crowded” edges.⁷ Such geometry combines the tetrahedral optical centers at angstrom scale and helical geometry of the overall shape of the NPs creating favorable conditions for strong photon-particle resonance. Exposure of human liver hepatocellular carcinoma cells (HepG2) to *L*-/*D*-Cys-stabilized graphene NPs reveals their general biocompatibility and a noticeable difference in the toxicity of the stereoisomers. Molecular dynamics simulations demonstrated that *D*-Cys-stabilized

graphene NPs have a stronger tendency to accumulate within the cellular membrane than *L*-Cys-stabilized graphene NPs. It was also found that CDots prepared from *D*-enantiomers of Cys and citric acid facilitate the growth and photosynthesis of plants more than those from *L*-enantiomers.¹⁶ Also, human bladder cancer cells treated with *L*-Cys-derived CDots showed up-regulated glycolysis, whereas *D*-Cys-derived CDots had no similar effect.¹⁷ *L*-lysine-based CDots dramatically remodeled amyloid beta-42 (A β 42) secondary structure and fibril morphologies and inhibited A β 42 cytotoxicity.¹⁸ CDots based on *L*- or *D*-glutamic acid reduced the production of blood glucose with *D*-CDots having a higher inhibitory efficiency than *L*-CDots.¹⁹ Cys-based CDots can also act as chiral templates to induce porphyrins to form chiral supramolecular assemblies.²⁰ However, chirality of nano-scale carbons remains broadly underutilized, poorly understood, and hardly optimized, especially in conjunction with other properties, such as PL, despite both of them being considered for biomedical applications. The implicit assumption is that these two properties can be independently maximized, which is not necessarily true.

Eco-friendly and low-cost hydrothermal synthesis is the most widely used method for the preparation of CDots.¹⁵ It also allows one to utilize a broad pool of starting materials (e.g., saccharides, amines, organic acids, and their derivatives).^{14,21,22} Chiral organic precursors are typically dissolved in a solvent and then heated in a Teflon-lined autoclave above the carbonization threshold. There are several separate reports on the influence of hydrothermal synthesis conditions (e.g., temperature, synthesis duration, and polarity of the solvent) on chiroptical and photoluminescent properties of CDots.^{17,23–25} However, to the best of our knowledge, there are no studies on the correlation between these optical properties and their dependencies on synthesis duration and temperature. These studies are required to develop CDots with optimal chiroptical and PL resonances.

The doping of CDots has been proven to increase their photoluminescence quantum yield (PL QY), which could be used to attain the combination of chirality and high PL simultaneously. The addition of boron (an electron acceptor) or nitrogen (an electron donor) into the chemical structure of nanocarbons could be accomplished by adding boric acid (BA) and nitrogen-containing organic molecules to the reaction mixture for hydrothermal reaction.^{26,27} Nitrogen and boron-doped CDots were reported for the hydrothermal process in the presence of citric acid, borax, and *p*-phenylenediamine,²⁸ which appeared to us quite an unusual finding considering low temperature of the synthesis. Hydrothermal method was also used for the fabrication of boron-doped CDots using ascorbic acid and BA as the precursors.²⁹

Boron-doped CDots were reported to have strong PL in the blue region upon ultraviolet excitation and an increase in the non-linear optical properties when compared with undoped CDots.²⁶ However, some studies reported that there is no significant boron doping observed in the CDots even after over 6 h in the reaction chamber, because the reaction conditions did not provide enough energy to incorporate the boron into the molecular structure of CDots.³⁰ Furthermore, several studies claimed the formation of boron nitride NPs in a hydrothermal reaction using BA and amino acid as a nitrogen source.^{31,32} Interestingly, the color of the produced dispersions and their optical properties were similar to those characterized as CDots and made from different amino acid hydrothermal reactions. These discrepancies between prior studies for chiral and other CDots make it essential to understand the chemistry of the products.

Here, we report the effect of hydrothermal synthesis duration and temperature on both chiroptical and PL properties of CDots derived from *L*- and *D*-Cys that will be abbreviated as *L*- and *D*-CDots, respectively. These notations reflect the chemical pathway for their preparation with understanding that they have multiple scale of chirality and not only the classical sp³ optical centers with tetrahedral geometry. We demonstrate that the NPs produced in the hydrothermal synthesis at 150°C have complex chemical structure due to the gradual dehydrogenation reactions leading to the formation of multiple functional groups. The degree of carbonization and content of aromatic groups increases with duration of the synthesis. The change in chemical structure leads to a decrease in chiroptical activity of CDots and an increase in their PL QY. The same trend occurs when the synthesis temperature increases for a fixed duration of the synthesis (4 h). We also demonstrated that the same reaction in the presence of BA leads to the formation of NPs those properties are very similar to that of CDots rather than of boron nitride NPs, as several published papers report.^{31,32}

2 | MATERIALS AND METHODS

2.1 | Materials

L-cysteine (*L*-Cys), *D*-cysteine (*D*-Cys), BA, NaOH, and Rhodamine 6G were purchased from Sigma-Aldrich. All the chemicals were of analytical grade and used without further treatment. The 0.22- μ m filter membranes were purchased from Sigma-Aldrich. Dialysis membranes with molecular weight cut-off of 1 kDa were obtained from Fisher Scientific. All solutions were prepared using ultrapure water (18.2 M Ω -cm) from a Milli-Q automatic ultrapure water system.

2.2 | Hydrothermal synthesis of *L*- and *D*-Cys-derived CDots

L-/*D*-Cys-derived CDots were synthesized by a one-step hydrothermal method. Briefly, 0.1 g of *L*- or *D*-Cys was sufficiently dissolved in 10 ml of water. Then, this solution was transferred to a 50-ml Teflon-sealed autoclave and heated at (i) 100/150/200/250°C for 4 h and (ii) 150°C for 1–20 h. If needed, the pH of the resulting solutions was adjusted to 7 using 0.1 M NaOH. Then, solutions were purified by passing through a 0.22- μ m filter membrane (see Figure S1) and dialysing against deionized water in a 1-kDa dialysis bag for 24 h. The pH of the NP dispersion after dialysis was found to be neutral, or the same pH as Millipore water, which means that unreacted cysteine and ultra-small molecular aggregates were removed. Also, all the samples were of 10 ml of volume, whereas the dialysis tank was 500 ml, which was also stirred to make the system homogenous. Thus, decreasing the concentration of solutes in about 50 times ensures better purification. As a result of hydrothermal synthesis and a further two-step purification procedure, ~10 mg of product was produced per 10 ml of purified solution.

2.3 | Hydrothermal synthesis in the presence of BA

The protocol is similar to that described in the previous section except for the addition of 0.67 g of BA to the Cys aqueous solution. The resultant mixture of Cys (0.1 g) and BA (0.67 g) was carefully mixed and put into a 50-ml Teflon-sealed autoclave. The rest of the procedure is identical to the described above.

2.4 | Characterization

UV-Vis absorption and PL spectroscopy were carried out using a Cary 8454 UV-Vis spectrophotometer and FluoroMax-3 fluorescence spectrophotometer (Horiba), respectively. PL QYs were measured using the comparison approach using Rhodamine 6G in ethanol (PL QY = 95%) as a standard. Transmission electron microscopy (TEM) was performed using a JEOL 3100R05 electron microscope operating at a beam voltage of 300 kV. X-ray photoelectron spectroscopy (XPS) was performed using a Kratos Axis Ultra XPS. Fourier-transform infrared (FTIR) spectroscopy was carried out using JASCO (FT/IR-4100) FTIR spectrometer. Nuclear magnetic resonance (NMR) spectroscopy was performed using Bruker Advance Neo 500 spectrometer. Circular

dichroism (CD) spectroscopy was carried out using a J-815 CD spectrometer (JASCO, Japan) operating under a N_2 flow of 5–8 l/min. Typical scanning parameters were as follows: scanning speed, 100 nm/min; data pitch, 1 nm; bandwidth, 1 nm, digital integration time, 2 sec; and one accumulation. The anisotropy factor (g -factor) was calculated according to the equation $g = CD / (32,980 \cdot Abs)$, where CD is the signal obtained from CD/DC channel (in mdeg) and Abs is the total absorbance. CD spectra were stopped at wavelengths where the hydrothermal voltage exceeded 400 V to avoid artifacts during acquisition.

3 | RESULTS AND DISCUSSION

Hydrothermal carbonization of *L*- or *D*-Cys was carried out under different temperatures and reaction times (Figure 1). At all other conditions being equal, the resulting *L*-CDots and *D*-CDots were very similar in structure and optical properties. Therefore, this manuscript focuses mainly on the *L*-CDots whereas additional details about *D*-CDots are provided in the supporting information.

The purification of as-synthesized samples is a vital step in the preparation of high-quality CDots because the excess of unreacted cysteine and small molecular species produced as byproducts could be responsible for the observed chemical and optical properties attributed to CDots. For example, recent 1H NMR spectroscopy studies on CDots made from tryptophan and other precursors showed that fluorescent aromatic molecules are indeed forming.³³ We extensively dialysed our samples in dialysis bags with different pore sizes (1 kDa and 3.5 kDa). When the duration of the hydrothermal carbonization reaction was less than 4 h, as-synthesized samples had CD spectra similar to those of untreated cysteine with some small shifts indicating the onset of dehydrogenation and oligomerization via C-C coupling. After dialysis in a

3.5 kDa bag, these samples became chiroptically silent because all the optically active species are at molecular scale for this stage of the reaction; they passed through the membrane and were found in the dialysis tank (Figure S2a). However, samples hydrothermally carbonized for over 4 h retained their CD spectrum after the dialysis both in 1 kDa and 3.5 kDa bags (Figure S2b,c). Given the fact that all the small soluble molecules were removed by dialysis, the CD spectra observed for products of the reactions lasting over 4 h originate from nano-scale particles.

1H NMR spectra of CDot samples thoroughly purified by exhaustive dialysis were collected for different durations of the hydrothermal reaction at 150°C. As the carbonization time increases from 2 to 4 and 20 h, the 1H NMR spectra experience distinct broadening (Figure 2). Concomitantly, the new peaks in the spectral windows of 7.5–6.5 ppm and 4.9–1.0 ppm also emerge. The increase of the NMR intensity in these two regions indicates the formation of aromatic (Ar) groups, and, in particular, peaks around 7 and 4 ppm indicate the formation of Ar–H and Ar–NH₂ functionalities. The formation of ether C–O–C cross-links as well as alcohol >C–OH groups are also likely. Based on these data, one can confidently conclude that CDots cannot be represented by a structural model assuming nearly perfect crystalline graphitic core at all reaction conditions, which would contradict the NMR data (Figure 2). Instead, CDots should be described as complex, extensively cross-linked NPs that acquire a dense, partially crystalline core only after extensive carbonization.

3.1 | Morphology and structure of the chiral CDots

The size distribution of CDots was calculated from the TEM images by counting ~100 NPs. *L*-CDots

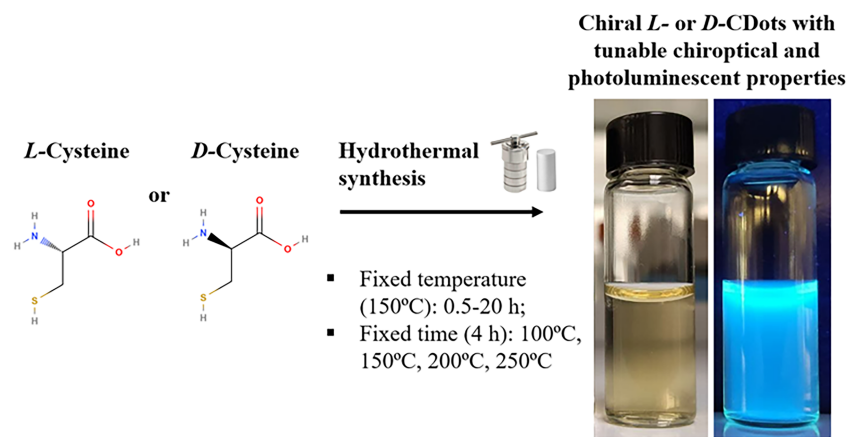


FIGURE 1 A schematic illustration for the preparation procedure of CDots by hydrothermal carbonization of *L*- or *D*-Cys. Inset: Photo image of the solutions of *L*-CDots synthesized for 4 h at 250°C. Left: Under daylight; right: Under 365-nm UV irradiation. CDots, carbon dots

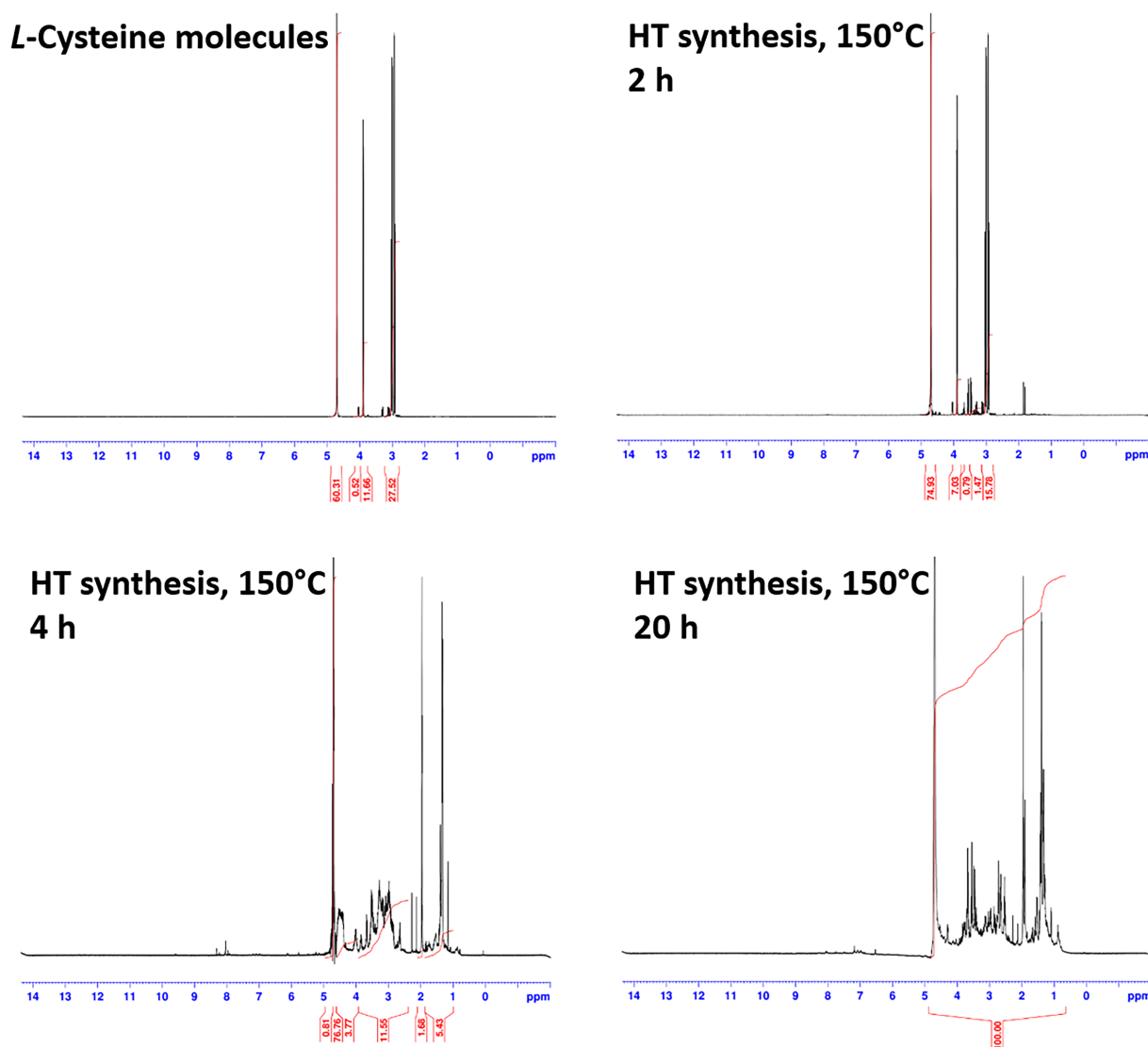


FIGURE 2 ^1H nuclear magnetic resonance spectra (D_2O) of untreated *L*-cysteine molecules, as well as samples obtained from a hydrothermal synthesis (150°C) for different durations of hydrothermal (HT) synthesis.

synthesized at 150°C for 4 and 20 h displayed an average size of 4.4 ± 0.5 and 5.3 ± 0.3 nm in diameter, respectively (Figure 3). Diameters of *D*-CDots synthesized at 150°C for 4 and 20 h were similar to those of corresponding *L*-CDots: 4.3 ± 0.3 and 5.2 ± 0.6 nm, respectively (see Figure S3). Thus, the longer duration of the hydrothermal synthesis results in a larger average diameter of CDots. In all cases discussed above, CDots were of uniform spherical morphology and fairly narrow size distribution. Notably, no NPs were detected when the synthesis duration was relatively short (<4 h) at 150°C , meaning these conditions were not enough to form the dense carbon cores. Similarly, samples synthesized for 4 h at 100°C displayed distinct crystallinity of the core but very faint contrast and it was challenging to assume the edge of these small particles/clusters to

determine their sizes (see Figure S4). Hydrothermal carbonization for 4 h at 250°C resulted in crystalline NPs with elongated geometry with long and short axes of ~ 13 and ~ 7 nm, respectively (see Figure S5). Quite expectedly based on NMR data (Figure 2), hydrothermal carbonization of cysteine is very sensitive to the synthesis temperature and duration, and higher temperatures and longer synthesis durations lead to NPs formation. It was reported previously that depending on the amino acids used as the precursors for hydrothermal synthesis of CDots, the sizes of resulting CDots can decrease or increase with increasing the temperature of the synthesis.²² The different variation trends of the diameters of CDots were explained with the different chemical structures of their precursors and their molecular weight.

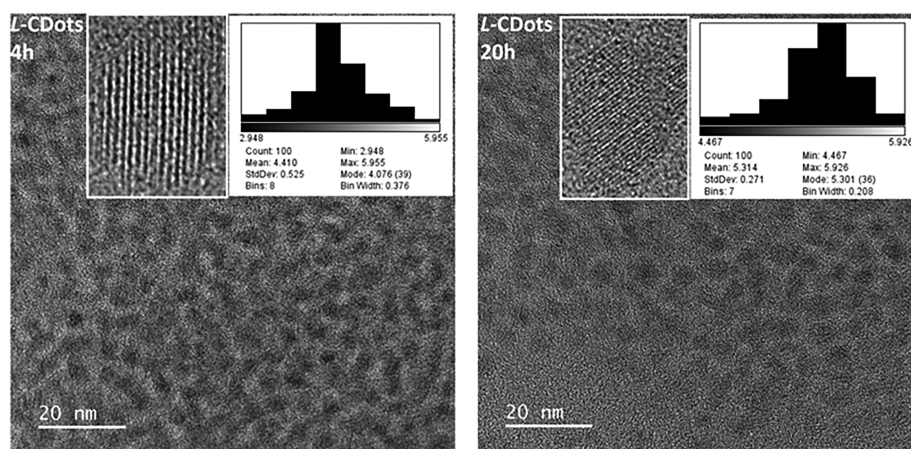


FIGURE 3 Transmission electron microscopy images of *L*-CDots synthesized for 4 (left) and 20 h (right) at 150°C. CDots, carbon dots

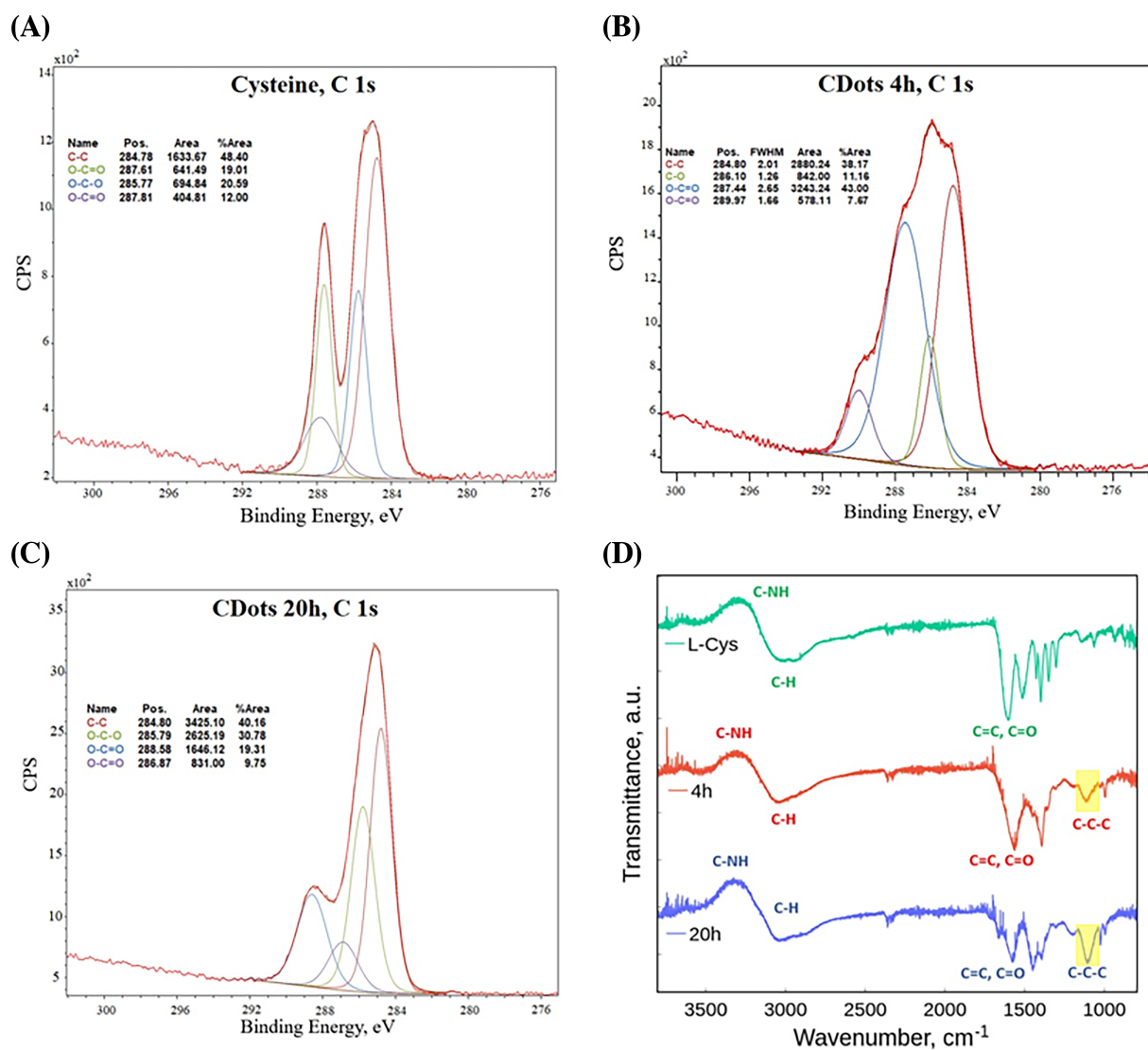


FIGURE 4 C 1s X-ray photoelectron spectroscopy spectra of (A) cysteine molecules, (B) *L*-CDots synthesized for 4 h at 150°C, and (C) *L*-CDots synthesized for 20 h at 150°C. (D) Fourier-transform infrared spectra of *L*-Cys molecules and *L*-CDots synthesized at 150°C for 4 and 20 h. CDots, carbon dots

XPS of CDots was compared with that of Cys (Figure 4A–C). From the XPS spectra of CDots synthesized for 4 h at 150 °C (Figure 4B), the C 1s peak consisted of peaks attributed to 284.80, 286.10, 287.44, and 289.97 eV peaks that corresponded to C–C, C–O, O–C=O, and O–C=O bonds, respectively,^{22,34} which agree very well with the conclusions from ¹H NMR study. The intensity and integrated area of the C–C bond peak increased with the increasing synthesis duration from 4 to 20 h (Figure 4B,C), indicating the increasing dominance of C–C bonds and a greater degree of carbonization.

FTIR spectrum also changes in the process of the hydrothermal reaction (Figure 4D). The FTIR spectra of *L*-/*D*-CDots agreed with previously published data on chiral carbon-based NPs.^{20,25,35} Using FTIR, it was determined that the peak at about 1195 cm⁻¹ includes sulfur, a C–S bond, and a C–O bond representing the cysteine chain.²³ As the CDots form, there is a peak at 1100 cm⁻¹ that is C–C–C bending with medium intensity.³⁶ The peak at 3000 cm⁻¹ corresponds to C–H, whereas the peak at 3300 cm⁻¹ is either C–OH or C–NH vibration.^{17,23} The peak at 1600 cm⁻¹ represents double bonds, specifically C=C and C=O.^{17,23} As the peak at about 3000 cm⁻¹ decreases with the reaction time, there are less C–H bonds in the structure. The FTIR results and XPS data both prove that as cysteine undergoes hydrothermal synthesis, C–H bonds are broken, the carbon-based skeleton of cysteine becomes stronger, and the amount of carbon increases as CDots emerge. We hypothesize that cysteine becomes more rigid as its skeletal bonds become

more prevalent and the C–H bonds and functional groups decrease in intensity. The surface of CDots is passivated with carboxyl groups.¹⁷

3.2 | Optical properties of cysteine-derived CDots

To study the influence of hydrothermal synthesis duration and temperature on the optical properties of CDots, their UV–Vis absorption (Figure 5) and PL emission spectra were recorded (Figure 6). Varying synthesis conditions, CDots samples have slightly different profiles of absorption spectra but all of them were located in 200- to 400-nm spectral region. Optical transitions in the 200–300 nm spectral range correspond to π - π^* transitions in sp²-hybridized carbon domains, whereas 300- to 400-nm range is attributed to n- π^* transitions.³⁷ As can be seen, there are no specific trends in CDots absorption spectra as the duration/temperature of their synthesis increases.

Analysis of PL properties of CDots shown that the shape and peak position of PL band (430 nm) remains the same as the duration/temperature of CDots synthesis increases. Under the excitation of the samples with 350-nm light, the position of the maximum PL intensity was at ~430 nm. Notably, the PL band maximum wavelength of CDots synthesized for 4 and 20 h at 150 °C experiences the redshift as the excitation wavelength increases from 260 to 400 nm (see Figure S6), which indicated the presence of lower energy states in accordance with the reported literature.³⁸ Also, both the increases

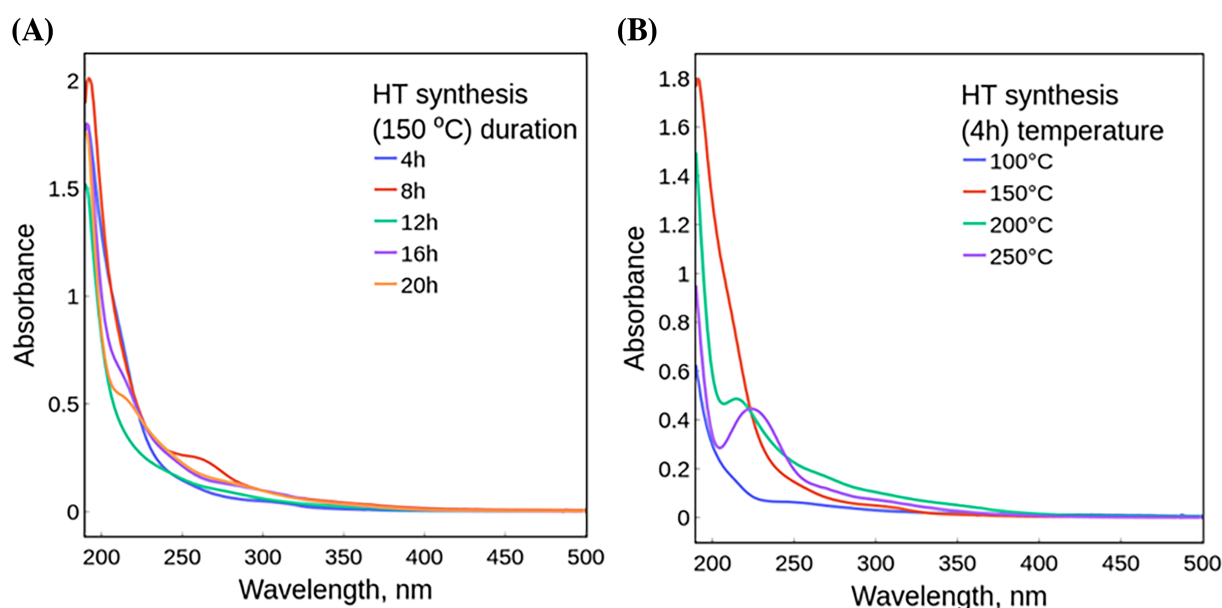


FIGURE 5 UV–Vis absorption spectra of *L*-CDots synthesized (A) at 150 °C for different durations and (B) for 4 h at different temperatures. Same UV–Vis profiles and intensities were observed for *D*-CDots. CDots, carbon dots; HT, hydrothermal

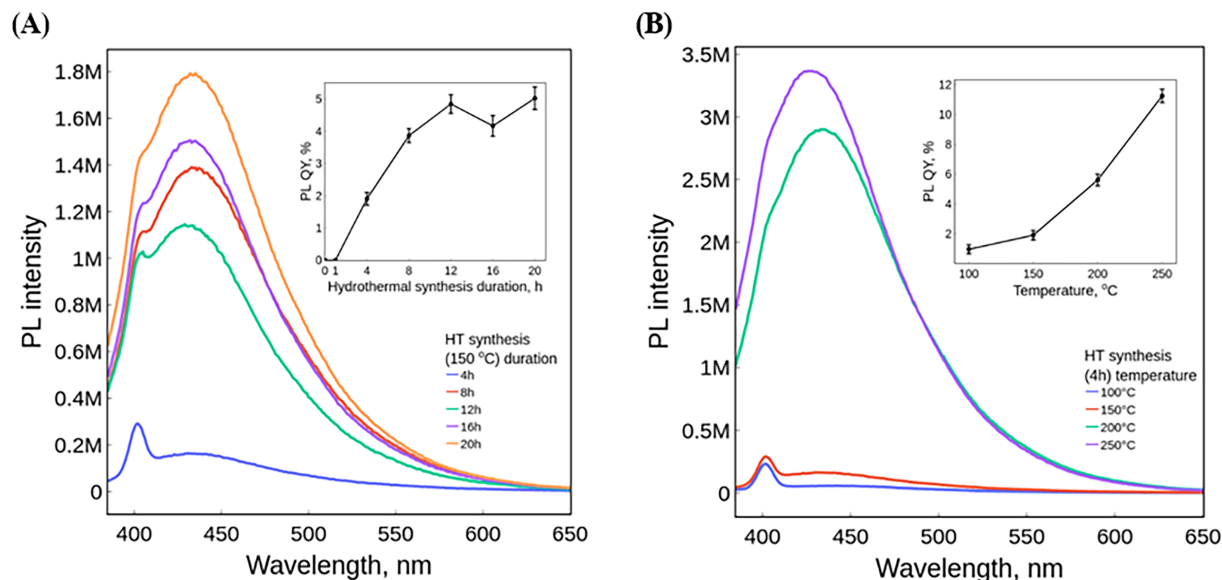


FIGURE 6 PL spectra ($\lambda_{\text{exc}} = 350$ nm) of *L*-CDots synthesized (A) at 150°C for different durations and (B) for 4 h at different temperatures. The dependencies of PL QY of *L*-CDots on the HT synthesis duration/temperature are shown in the insets of (A) and (B), respectively. Same emission profiles and intensities, as well as PL QYs were observed for *D*-CDots. CDots, carbon dots; HT, hydrothermal; PL QYs, photoluminescence quantum yields

of (1) synthesis duration at a fixed temperature and (2) synthesis temperature at a fixed time lead to the increase in the PL QY of CDots (Figure 6A,B, inserts). However, the trends of the PL QY increase are different. In the first case, PL QY was increasing faster but reached the saturation of $\sim 5\%$ after 12 h of synthesis. In the second case, the synthesis temperature increases from 100°C to 250°C followed by the PL QY rapid increase, which also allowed to reach higher PL QY values with $\sim 11\%$ efficiency. In both cases, the PL QY increase could be associated with the gradually increasing crystallinity of the carbon cores in CDots, which also had been observed for other types of nanostructures.³⁹ And the difference between the two conditions could be explained by the different dynamics of the crystal growth/crystallization, which occur faster at higher temperatures.

3.3 | Chiroptical properties of cysteine-derived CDots

Besides CD spectra, for quantitative analysis of the optical activity of liquid solutions and dispersions, the dissymmetry factor (*g*-factor) is used, which is defined as $g = \Delta\epsilon/\epsilon = (\epsilon_L - \epsilon_R)/(\epsilon_L + \epsilon_R)$, where $\Delta\epsilon$ is molar CD, ϵ is molar extinction, and ϵ_L and ϵ_R are the molar extinction coefficients for left- and right-handed circularly polarized light, respectively (see Section 2 for more details). The dissymmetry *g*-factor is independent of sample concentration and cell path length, which is

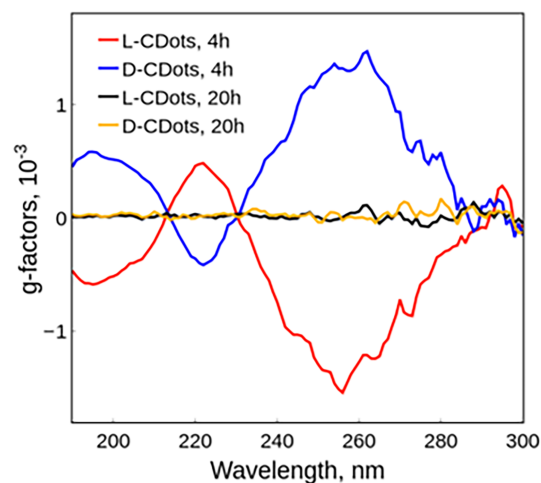


FIGURE 7 *g*-factor spectra of *L*-/*D*-CDots synthesized at 150°C for 4 and 20 h. CDots, carbon dots

important for the comparative studies of samples with variable concentrations.

The mirror-imaged CD (see Figure S7) and *g*-factor (Figure 7) spectra of *L*- and *D*-CDots synthesized for 4 h at 150°C indicate the successful synthesis of CDots with chiroptical activity. The further increase in synthesis duration to 20 h led to the CDots that are chiroptically silent (Figures 7 and S7).

Analysis of the effect of synthesis duration and temperature on chiroptical activity of CDots allowed to establish that decomposition of Cys to CDots is accompanied

by the dramatic drop of g -factor at ~ 4 h of reaction (Figure 8). Prolonged synthesis duration and increased reaction temperature decreased g -factor value even further and caused the disappearance of chiroptical activity after 12 h of reaction (Figure 8). We believe that this phenomenon occurs due to the increased carbonization and the loss of atomic-scale chirality on the surface of CDots as the optical center of Cys decomposes in the course of the hydrothermal synthesis. High symmetry of carbon crystal lattice also reduces nanoscale chirality of the CDots, albeit retaining the preferential non-spherical shapes of the particles. Longer duration and higher temperatures also facilitate “racemization” of CDots under

harsh conditions.³⁷ The PL QY trend is the opposite with light emission (Figure 6) improving with both reaction parameters, degree of carbonization, and increased crystallinity of CDots (Figure 3). The same trends were reported for semiconductor CdSe NPs.³⁹

3.4 | Hydrothermal synthesis of cysteine-derived CDots in the presence of boric acid

The doping of CDots could be potentially used to increase their PL QY and chiroptical activity at the same time.

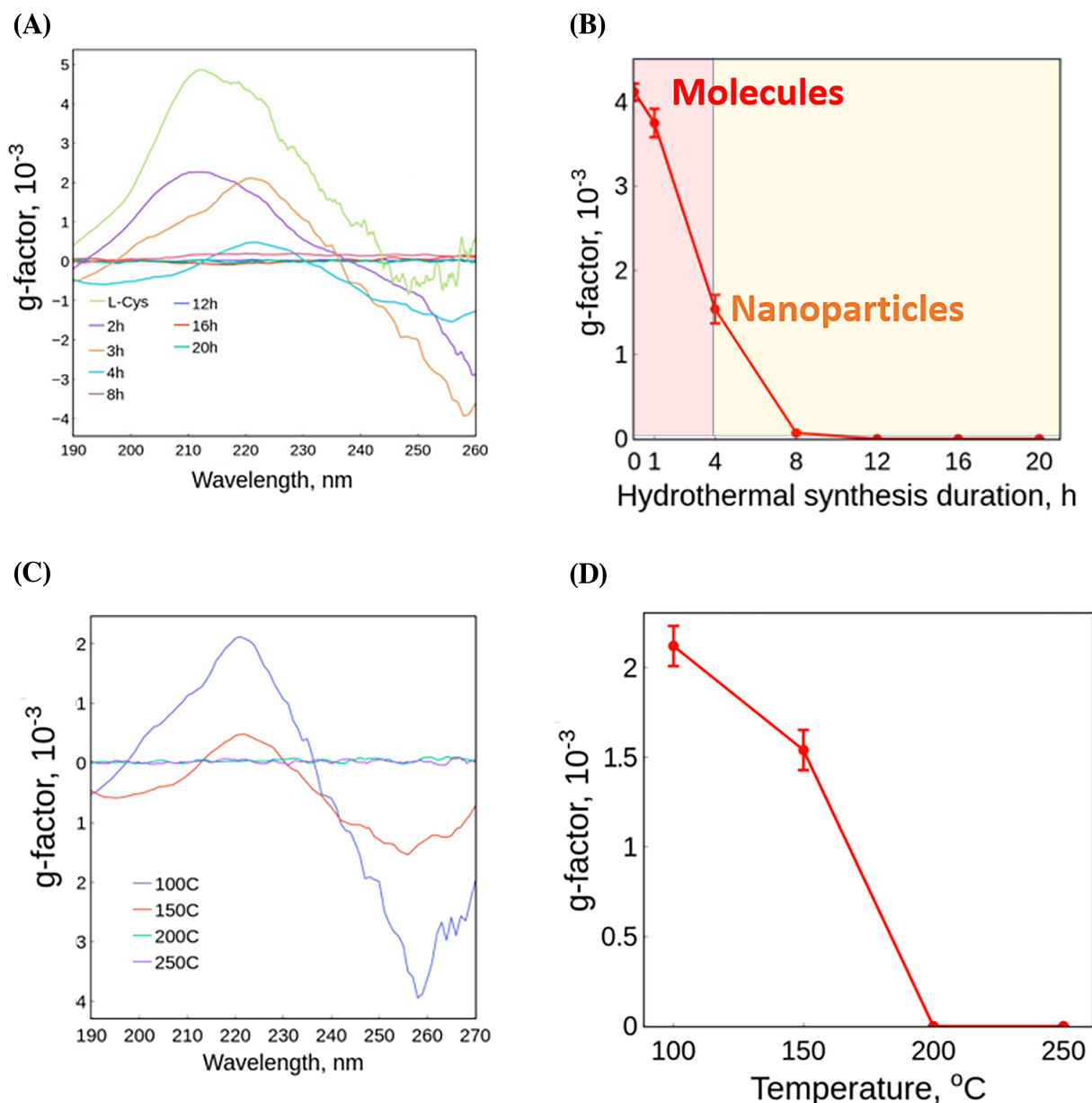


FIGURE 8 (A) g -factor spectra and (B) g -values of L -CDots synthesized at 150°C for different durations and (C) g -factor spectra and (D) g -values of L -CDots synthesized for 4 h at different temperatures. CDots, carbon dots

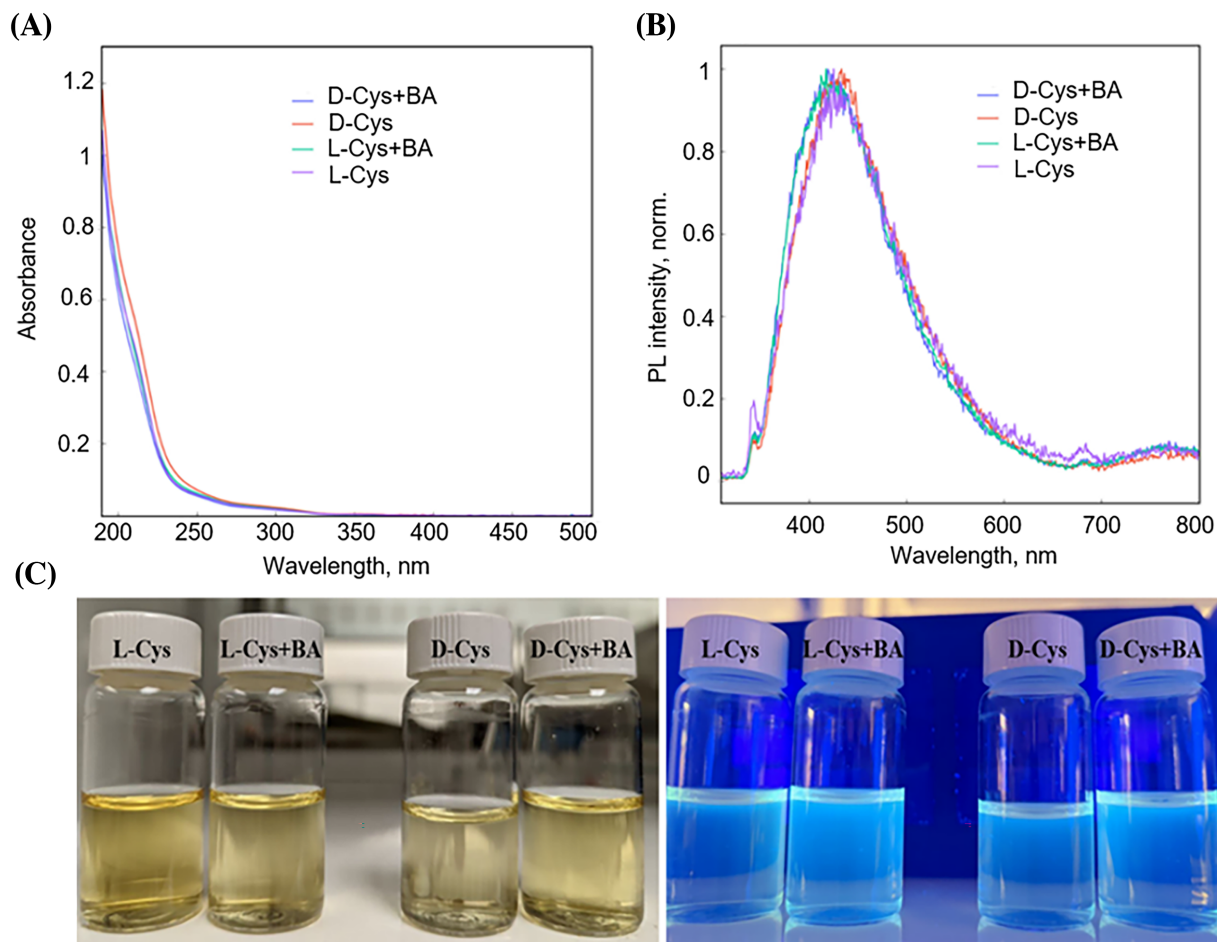


FIGURE 9 (A) UV-Vis absorption and (B) PL spectra of *L-/D*-CDots synthesized with and without boric acid at 150°C for 4 h. (C) Photo image of corresponding solutions of CDots. Left: Under daylight; right: Under 365-nm UV irradiation. BA, boric acid; CDots, carbon dots; PL, photoluminescent

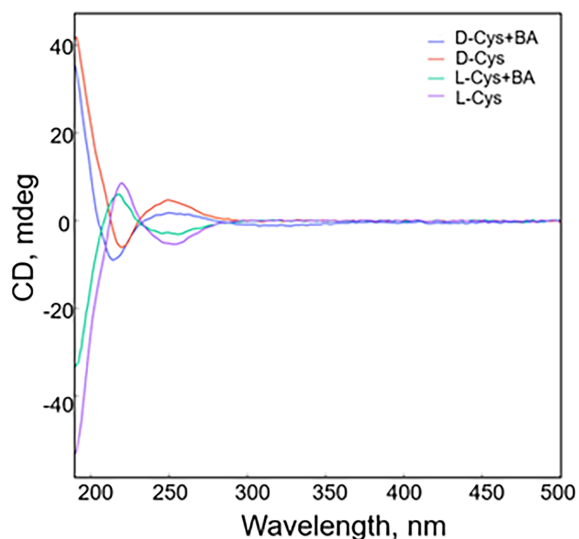


FIGURE 10 CD spectra of *L-* and *D-*CDots synthesized with and without boric acid at 150°C for 4 h. BA, boric acid; CD, circular dichroism; CDots, carbon dots

Here, we attempted to synthesize chiral boron-doped CDots with cysteine and BA as precursors (see Section 2). We found that absorbance (Figure 9A), PL (Figure 9B), CD (Figure 10), and FTIR (Figure S8) spectra of samples prepared with and without BA are nearly identical. This experimental fact indicates that BA has little to no effect on the formation of CDots and that the chiral boron nitride NPs are unlikely to form in this reaction pathway. Unlike previous reports,^{31,32} our analysis concludes the exclusive formation of CDots rather than boron-doped carbonization products. It is also critical to state that our experiments included controls of BA, *D*-Cys, and *L*-Cys, so that we could analyze and compare all aspects of the experiments.

4 | CONCLUSION

We synthesized CDots by one-step hydrothermal method from Cys precursor, studied their chemical structure and

optical properties. We found that the CDots are the products of the gradual dehydrogenation and carbonization reaction with intermediate oligomeric species. They are likely to produce 'hairy' interface with a variety of carbon oxidation states as revealed by the NMR data in Figure 2. Due to the gradual increase of the crystallinity in the core and progressive racemization, the PL QY of CDots has a direct correlation with the synthesis duration and temperature, whereas g-factors have an inverse one. The similar hydrothermal reaction with thermal decomposition of amino acid in the presence of BA leads to the formation of CDots rather than to boron nitride NPs or boron-doped carbon particle. These findings will facilitate the synthesis of chiral carbon-based and other NPs with application-optimized chemical, chiroptical, and PL properties.

ACKNOWLEDGMENTS

The central part of this work was supported by the Vannevar Bush DoD Fellowship to N.A.K. titled "Engineered Chiral Ceramics" ONR N000141812876 and MURI from the Office of Naval Research (MURI N00014-20-1-2479). This work was also partially supported by MURI N00014-18-1-2497. The authors are also grateful for dedicated funding from the DEI Initiative UM College of Engineering for student travel. The authors acknowledge the financial support of the University of Michigan College of Engineering and National Science Foundation (NSF) grant #DMR-0723032 and technical support on the TEM characterization using JEOL 3100R05 from the Michigan Center for Materials Characterization. The authors also acknowledge the financial support of the University of Michigan College of Engineering and NSF grant #DMR-0420785 and technical support on the XPS analysis from the Michigan Center for Materials Characterization. This work was also supported by NSF grants 1830886 and 1856515, Air Force Office of Scientific Research (AFOSR) grant FA9550-18-1-0417, Department of Defense (DoD) grant W911NF1810472, and National Nuclear Security Administration (NNSA) award DE-NA0004007. The work was partly supported by the Laboratory Directed Research and Development program at Sandia National Laboratories, a multimission laboratory managed and operated by National Technology and Engineering Solutions of Sandia, LLC, a wholly owned subsidiary of Honeywell International, Inc., for the U.S. Department of Energy's NNSA under Contract No. DE-NA-0003525. The authors also acknowledge the financial support of the NSF CREST #2112595.

DATA AVAILABILITY STATEMENT

Additional supporting information may be found in the online version of this article at the publisher's website.

Supplementary characterization of CDots and materials obtained during the hydrothermal synthesis of amino acids in the presence of boric acid.

The data that support the findings of this study are available from the corresponding author upon request.

ORCID

Anastasia Visheratina  <https://orcid.org/0000-0001-7839-6496>

Nicholas A. Kotov  <https://orcid.org/0000-0002-6864-5804>

REFERENCES

1. Ma W, Xu L, de Moura AF, et al. Chiral inorganic nanostructures. *Chem Rev.* 2017;117:12. doi:10.1021/acs.chemrev.6b00755
2. Visheratina A, Kotov NA. Inorganic nanostructures with strong chiroptical activity. *CCS Chem.* 2020;583-604.
3. Ma W, Xu L, Wang L, Xu C, Kuang H. Chirality-based biosensors. *Adv Funct Mater.* 2018;1805512. doi:10.1002/adfm.201805512
4. Gogoi A, Mazumder N, Konwer S, Ranawat H, Chen NT, Zhuo GY. Enantiomeric recognition and separation by chiral NPs. *Molecules.* 2019;24(6):1007. doi:10.3390/molecules24061007
5. Kumar J, Thomas KG, Liz-Marzán LM. Nanoscale chirality in metal and semiconductor NPs. *Chem Commun.* 2016;52(85):12555-12569. doi:10.1039/C6CC05613J
6. Sanchez-Valencia JR, Dienel T, Gröning O, et al. Controlled synthesis of single-chirality carbon nanotubes. *Nature.* 2014;512(7512):61-64.
7. Suzuki N, Wang Y, Elvati P, et al. Chiral graphene quantum dots. *ACS Nano.* 2016;10(2):1744-1755. doi:10.1021/acsnano.5b06369
8. Zheng W-W, Hsieh Y-H, Chiu Y-C, Cai S-J, Cheng C-L, Chen C. Organic functionalization of ultradispersed nanodiamond: synthesis and applications. *J Mater Chem.* 2009;19(44):8432-8441.
9. Baker SN, Baker GA. Luminescent carbon nanodots: emergent nanolights. *Angew Chem Int Ed.* 2010;49(38):6726-6744.
10. Zheng XT, Ananthanarayanan A, Luo KQ, Chen P. Glowing graphene quantum dots and carbon dots: properties, syntheses, and biological applications. *Small.* 2015;11(14):1620-1636.
11. Chahal S, Macairan J-R, Yousefi N, Tufenkji N, Naccache R. Green synthesis of carbon dots and their applications. *RSC Adv.* 2021;11(41):25354-25363.
12. Essner JB, Baker GA. The emerging roles of carbon dots in solar photovoltaics: a critical review. *Environ Sci Nano.* 2017;4(6):1216-1263.
13. Tian Z, Zhang X, Li D, et al. Full-color inorganic carbon dot phosphors for white-light-emitting diodes. *Adv Opt Mater.* 2017;5(19):1700416.
14. Hesari M, Ding Z. A perspective on application of carbon quantum dots in luminescence immunoassays. *Front Chem.* 2020;8:946.
15. Döring A, Ushakova E, Rogach AL. Chiral carbon dots: synthesis, optical properties, and emerging applications. *Light Sci Appl.* 2022;11(1):75. doi:10.1038/s41377-022-00764-1

16. Zhang M, Hu L, Wang H, et al. One-step hydrothermal synthesis of chiral carbon dots and their effects on mung bean plant growth. *Nanoscale*. 2018;10(26):12734-12742.
17. Li F, Li Y, Yang X, et al. Highly fluorescent chiral N-S-doped carbon dots from cysteine: affecting cellular energy metabolism. *Angew Chem*. 2018;130(9):2401-2406.
18. Malishev R, Arad E, Bhunia SK, et al. Chiral modulation of amyloid beta fibrillation and cytotoxicity by enantiomeric carbon dots. *Chem Commun*. 2018;54(56):7762-7765.
19. Zhang M, Wang H, Wang B, et al. Maltase decorated by chiral carbon dots with inhibited enzyme activity for glucose level control. *Small*. 2019;15(48):1901512.
20. Liu X, Lu J, Chen J, et al. Chiral self-assembly of porphyrins induced by chiral carbon dots. *Front Chem*. 2020;8:670.
21. Sharma A, Das J. Small molecules derived carbon dots: synthesis and applications in sensing, catalysis, imaging, and biomedicine. *J Nanobiotechnol*. 2019;17(1):1-24.
22. Pei S, Zhang J, Gao M, Wu D, Yang Y, Liu R. A facile hydrothermal approach towards photoluminescent carbon dots from amino acids. *J Colloid Interface Sci*. 2015;439:129-133.
23. Hu L, Sun Y, Zhou Y, et al. Nitrogen and sulfur co-doped chiral carbon quantum dots with independent photoluminescence and chirality. *Inorg Chem Front*. 2017;4(6):946-953. doi:10.1039/C7QI00118E
24. Đorđević L, Arcudi F, D'Urso A, et al. Design principles of chiral carbon nanodots help convey chirality from molecular to nanoscale level. *Nat Commun*. 2018;9(1):1-8.
25. Wei Y, Chen L, Wang J, Liu X, Yang Y, Yu S. Investigation on the chirality mechanism of chiral carbon quantum dots derived from tryptophan. *RSC Adv*. 2019;9(6):3208-3214.
26. Bourlinos AB, Trivizas G, Karakassides MA, et al. Green and simple route toward boron doped carbon dots with significantly enhanced non-linear optical properties. *Carbon N Y*. 2015;83:173-179.
27. Jahan S, Mansoor F, Naz S, Lei J, Kanwal S. Oxidative synthesis of highly fluorescent boron/nitrogen co-doped carbon nanodots enabling detection of photosensitizer and carcinogenic dye. *Anal Chem*. 2013;85(21):10232-10239.
28. Liu Y, Li W, Wu P, et al. Hydrothermal synthesis of nitrogen and boron co-doped carbon quantum dots for application in acetone and dopamine sensors and multicolor cellular imaging. *Sens Actuators B*. 2019;281:34-43. doi:10.1016/j.snb.2018.10.075
29. Wang Z-X, Yu X-H, Li F, et al. Preparation of boron-doped carbon dots for fluorometric determination of Pb(II), Cu(II) and pyrophosphate ions. *Microchimica Acta*. 2017;184(12):4775-4783. doi:10.1007/s00604-017-2526-3
30. Choi Y, Kang B, Lee J, et al. Integrative approach toward uncovering the origin of photoluminescence in dual heteroatom-doped carbon nanodots. *Chem Mater*. 2016;28(19):6840-6847.
31. Kong Y, He Y, Zhou J, Zhong S, Song G. Amino acids as the nitrogen source to synthesize boron nitride quantum dots for fluorescence turn-off-on detection of ascorbic acid. *Chem Select*. 2020;5(13):3828-3834. doi:10.1002/slct.202000602
32. Kainthola A, Bijalwan K, Negi S, Sharma H, Dwivedi C. Hydrothermal synthesis of highly stable boron nitride NPs. *Mater Today Proc*. 2020;28:138-140. doi:10.1016/j.matpr.2020.01.452
33. Bartolomei B, Bogo A, Amato F, Ragazzon G, Prato M. Nuclear magnetic resonance reveals molecular species in carbon nanodot samples disclosing flaws. *Angew Chem Int Ed*. 2022;61(20):e202200038. doi:10.1002/anie.202200038
34. Das A, Kundelev EV, Vedernikova AA, et al. Revealing the nature of optical activity in carbon dots produced from different chiral precursor molecules. *Light Sci Appl*. 2022;11(1):92. doi:10.1038/s41377-022-00778-9
35. Visheratina AK, Purcell-Milton F, Serrano-García R, et al. Chiral recognition of optically active CoFe₂O₄ magnetic NPs by CdSe/CdS quantum dots stabilised with chiral ligands. *J Mater Chem C Mater*. 2017;5(7):1692-1698.
36. Silverstein RM, Webster FX, Kiemle DJ. *Spectrometric Identification of Organic Compounds*. 7th ed. John Wiley & Sons, Inc.; 2005. doi:10.1021/ed039p546
37. Ragazzon G, Cadranel A, Ushakova EV, et al. Optical processes in carbon nanocolloids. *Chem*. 2021;7(3):606-628. doi:10.1016/j.chempr.2020.11.012
38. Li X, Zhang S, Kulinich SA, Liu Y, Zeng H. Engineering surface states of carbon dots to achieve controllable luminescence for solid-luminescent composites and sensitive Be²⁺ detection. *Sci Rep*. 2015;4(1):4976. doi:10.1038/srep04976
39. Purcell-Milton F, Visheratina AK, Kuznetsova VA, Ryan A, Orlova AO, Gun'ko YK. Impact of shell thickness on photoluminescence and optical activity in chiral CdSe/CdS core/shell quantum dots. *ACS Nano*. 2017;11(9):9207-9214. doi:10.1021/acsnano.7b04199

SUPPORTING INFORMATION

Additional supporting information can be found online in the Supporting Information section at the end of this article.

How to cite this article: Visheratina A, Hesami L, Wilson AK, et al. Hydrothermal synthesis of chiral carbon dots. *Chirality*. 2022; 34(12):1503-1514. doi:10.1002/chir.23509